View Article Online
View Journal

Faraday Discussions

Accepted Manuscript

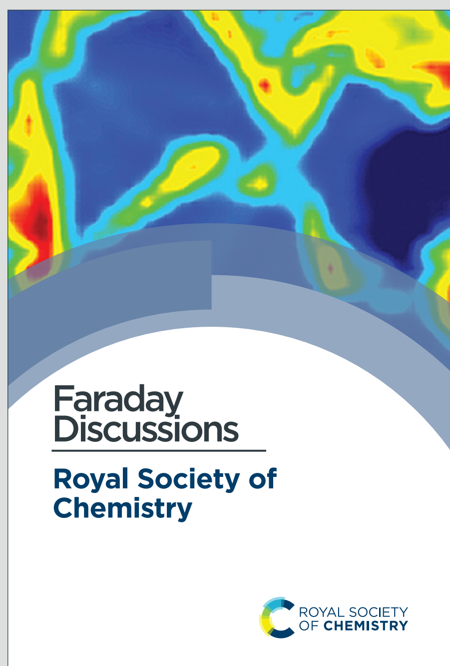

This is an Accepted Manuscript, which has been through the Royal Society of Chemistry peer review process and has been accepted for publication.

Accepted Manuscripts are published online shortly after acceptance, before technical editing, formatting and proof reading. Using this free service, authors can make their results available to the community, in citable form, before we publish the edited article. We will replace this Accepted Manuscript with the edited and formatted Advance Article as soon as it is available.

You can find more information about Accepted Manuscripts in the Information for Authors.

Please note that technical editing may introduce minor changes to the text and/or graphics, which may alter content. The journal's standard Terms & Conditions and the Ethical guidelines still apply. In no event shall the Royal Society of Chemistry be held responsible for any errors or omissions in this Accepted Manuscript or any consequences arising from the use of any information it contains.

This article can be cited before page numbers have been issued, to do this please use: X. Li, S. Gross, T. Haunold, M. Jang, M. Zukalová, M. Jindra, J. E. Olszówka, Y. Lei, S. Vajda and G. Rupprechter, *Faraday Discuss.*, 2026, DOI: 10.1039/D5FD00152H.

ROYAL SOCIETY OF CHEMISTRY

www.rsc.org/faraday_d

Probing the Structure of D_2O Ice Layers on ALD-Grown ZrO_2, Al_2O_3 and TiO_2 Thin Films by Sum Frequency Generation (SFG) Spectroscopy

View Article Online
DOI: 10.1039/D5FD00152H

Xia Li[1*], Susanne Gross[1], Thomas Haunold[1], Moon-Hyung Jang[2], Marketa Zukalova[3], Martin Jindra[3], Joanna E. Olszówka[4], Yu Lei[2], Štefan Vajda[4], and Günther Rupprechter[1*]

1. Institute of Materials Chemistry, TU Wien, Vienna 1060, Austria.
2. Department of Chemical and Materials Engineering, University of Alabama in Huntsville, Huntsville, AL, 35899, USA.
3. Department of Electrochemical Materials, J. Heyrovsky Institute of Physical Chemistry, Dolejškova 2155/3, 182 00 Prague 8, Czech Republic.
4. Department of Nanocatalysis, J. Heyrovsky Institute of Physical Chemistry, Prague, Czech Republic.

Open Access Article. Published on 16 Dezember 2025. Downloaded on 04.04.2026 08:28:47.
This article is licensed under a Creative Commons Attribution 3.0 Unported Licence.

Keywords Sum frequency generation, D_2O, Ice, Oxides, Atomic layer deposition (ALD), surface/interface, hydrogen bonding

Abstract Sum frequency generation (SFG) spectroscopy was applied to investigate D_2O adsorption on atomic layer deposition (ALD)–grown Al_2O_3, ZrO_2, and TiO_2 films at 94 ± 1 K. Film composition and thickness were characterized by ellipsometry and X-ray photoelectron spectroscopy (XPS). Additional SFG measurements were conducted on the SiO_2/Si wafer and on a CoO film prepared by oxidizing Co foil. At D_2O exposure below 3 000 L, the spectra were dominated by interfacial features originating from the ice-oxide interface. These spectra exhibited a weak, broad O–D stretching band (OD_3) centered at 2650 cm^{-1}, attributed to water molecules hydrogen-bonded to the oxide surface; this assignment was supported by the absence of the OD_3 feature on the SiO_2/Si substrate. A sharp peak at 2730 cm^{-1} was also observed and assigned to the "free" O–D stretch (non-hydrogen-bonded with any neighboring molecule) of surface D_2O molecules pointing into the vapor phase. Upon increasing D_2O exposure, both the OD_3 and "free" OD bands decreased in intensity and were replaced by weakly hydrogen-bonded OD_2 and strongly hydrogen-bonded OD_1 modes associated with the ice-vapor interface. As the exposure increased further, the OD_2 and OD_1 bands shifted to lower wavenumbers (2310 to 2284 cm^{-1}) and became stronger, with the OD_1 mode exhibiting a larger red shift and more pronounced intensity enhancement. No significant differences in water structure were observed on the Al_2O_3, ZrO_2, and CoO films at the ice-vapor interfaces, apart from an approximately fivefold reduction in intensity on CoO, which is attributed to signal scattering from the rough CoO film/Co foil surface. However, when D_2O exposure reached ≥30 000 L, the OD_1 band on the TiO_2 surfaces decreased substantially in intensity and shifted to much lower wavenumbers (2065 cm^{-1} at 30 000 L;

Faraday Discussions Accepted Manuscript

2030 cm^{-1} at 102 000 L) than on Al_2O_3 (2283 cm^{-1} at 90 000 L), ZrO_2 (2293 cm^{-1} at 30 000 L), and CoO (2284 cm^{-1} at 900 000 L), indicating specific hydrogen-bonding interactions on the TiO_2 surface.

View Article Online
DOI: 10.1039/D5FD00152H

Introduction

Water plays a pivotal role in numerous chemical, physical and biological processes, both in nature and industry. With the growing global concern over energy generation and environmental pollution associated with the extensive use of non-renewable fossil fuels, the development of clean and efficient hydrogen (H_2) production technologies has become increasingly important. Among various approaches, water serves as a direct key source for H_2 such as water-gas shift (WGS) ($CO+H_2O \leftrightarrow CO_2+H_2$, ΔH=-41.2 kJ/mol)[1-5] and methanol steam reforming (MSR, $CH_3OH+H_2O \leftrightarrow CO_2+3H_2$, ∆H= +49.7 kJ/mol)[6-8], which are typically catalyzed by oxide-supported transition metals, or water serving as a promoter affecting activity and/or selectivity[9-11].

Metal oxides play a crucial role in these processes, particularly in the activation and dissociation of H_2O. Among commonly used supports such as CeO_2, Al_2O_3, ZrO_2, or TiO_2, the catalytic activity varies significantly due to differences in strong metal-support interaction (SMSI)[3, 4, 12, 13]. For instance, in the WGS reaction, Pt-Ni bimetallic catalysts supported on reducible or partially reducible oxides (CeO_2, TiO_2 and HSA-ZrO_2) exhibit higher activity than those supported on non-reducible oxides (γ-Al_2O_3, SiO_2 and LSA-ZrO_2)[3]. Similarly, for Cu-based catalysts in WGS[5], CO conversion between 320 and 360 °C decreases in the order of Cu/CeO_2 > Cu/MgO > Cu/ZrO_2 > Cu/Al_2O_3.

In the case of MSR using Pd-based catalysts, Takezawa and co-workers[13] compared various oxide supports and found that Pd/ZrO_2 exhibits excellent MSR activity and selectivity, second only to Pd/ZnO. The overall activity order of the oxide supports was ZnO> ZrO_2> Nd_2O_3> La_2O_3> Al_2O_3> Nd_2O_5> SiO_2. These observations clearly demonstrate the significant influence of the oxide support on catalytic performance.

Furthermore, water-oxide interactions are of great importance across various fields, including corrosion, catalysts, geochemistry, atmospheric chemistry, biology, and materials science, as illustrated in numerous review articles[14-17]. Therefore, elucidating the structure and behavior of interfacial water on different oxide surfaces is of particular interest.

However, distinguishing between monolayer and multilayer water structures on oxide surfaces remains challenging, as several traditional surface characterization techniques have inherent limitations[16]. Electron spectroscopies are hindered by the insulation of bulk water, which causes surface charging. Scanning tunneling microscopy can only be applied to films thinner than three molecular layers to avoid conductivity issues. Vibrational spectroscopic techniques, such as surface infrared spectroscopy, are well-suited for probing adsorbate geometry and dynamics[18], however, infrared measurements generally average over both bulk and surface contributions[16].

Open Access Article. Published on 16 Dezember 2025. Downloaded on 04.04.2026 08:28:47.
This article is licensed under a Creative Commons Attribution 3.0 Unported Licence.

Faraday Discussions Accepted Manuscript

View Article Online
DOI: 10.1039/D5FD00152H

Sum frequency generation (SFG) spectroscopy[19-22], a second-order nonlinear optical technique, has proven particularly effective for probing molecular vibrations at surfaces/interfaces[22-26], as the adjacent bulk phases do not contribute to the signal. Using this method, numerous studies have investigated water structures at a variety of interfaces, including water-air interface[27], water-metal interfaces[28], aqueous-mineral interface (e.g., SiO_2, Al_2O_3, CaF_2, and TiO_2)[29, 30], graphene-water[31-33], graphene oxide-water[34], and ultrathin Au film-water (2 nm or less) systems[35].

Ice, a hydrogen-bonded solid form of water, consists of water molecules held together by a tetrahedral hydrogen bonding network. However, ice is structurally complex, exhibiting as many as 17 crystalline polymorphs and 2 amorphous solids[36]. Its high vapor pressure (above 170 K, $>10^{-3}$ Pa[36]) and polymorphism make it a challenging subject in surface science. Shen and coworkers[37] first reported conventional SFG spectra of the basal face of single-crystalline ice I_h at 170-270 K in 2001. Subsequently, ice at various surfaces and interfaces (e.g., air, SiO_2, Pt(111)) has been extensively studied using SFG[36, 38-40].

A single water layer can readily form at low temperatures (< 150 K) under UHV conditions[16]. Somorjai and coworkers[39] demonstrated that ice films (< 30 ML thickness) grown on Pt(111) at 120-137 K exhibit ferroelectric ordering —a term loosely describing a net polar orientation of water molecules within the ice films. Classified based on the number of hydrogen bonding donors (D) and acceptors (A), below 200 K, the topmost ice surface becomes increasingly crystalline, where double donor-double acceptor DDAA-type water molecules break one hydrogen bond and rearrange into the hexagonal H-bond network, forming single donor-double acceptor DAA-type water species[40]. At the ice-sapphire interface, a sharp peak at 3100 cm^{-1} has been attributed to the OH stretching of highly ordered water molecules in ice I_h crystals[31]. In contrast, the ice structure adjacent to graphite shows little to no temperature dependence between 261 and 273 K. Molecular dynamics (MD) simulations have further suggested that monolayer ice confined inside graphene nanocapillaries forms a puckered zigzag structure[41].

In this study, we investigated D_2O ice (I_h) adsorption at 93–95 K, a relatively low temperature, under various exposures rather than temperature variations, on three atomic layer deposition (ALD) oxide films—Al_2O_3, ZrO_2, and TiO_2—using a Si wafer as the substrate (as reported in refs[42, 43]). Water adsorption on pure Si and on a CoO film supported on an unpolished Co foil are used as references. Water exposure is controlled by adjusting both the D_2O vapor pressure and exposure time.

Results and discussion

Prior to the discussion of the results, the procedure of ALD sample preparation and characterization is briefly illustrated in **Figure 1**. All atomic layer deposition (ALD) oxide films (Al_2O_3, TiO_2, ZrO_2) were

Open Access Article. Published on 16 Dezember 2025. Downloaded on 04.04.2026 08:28:47.

This article is licensed under a Creative Commons Attribution 3.0 Unported Licence.

Faraday Discussions Accepted Manuscript

grown on Si(100) wafers (size: 7x7 mm^2) and measured thickness by ellipsometry. After transferring into the XPS/LEIS-UHV 1 system (Austria), the samples were thoroughly cleaned by oxidation (1x10^{-6} mbar O_2, 923 K, 30 min) and reduction (1x10^{-6} mbar H_2, 923 K, 30 min) to remove potential contaminations introduced by air exposure. All XPS measurements were performed at room temperature (RT) under UHV conditions. Subsequently, the ALD samples were transferred in air to the UHV-compatible SFG cell (SFG-UHV 2). Again, accounting for air exposure, the samples were oxidized (1x10^{-5} mbar, 600 K, 60 min) before SFG measurements to remove any remaining contaminants. To ensure clean surfaces, SFG spectra of the pure oxide films were recorded first. Finally, SFG spectra were obtained at 93-95 K after dosing water at the same temperature.

View Article Online
DOI: 10.1039/D5FD00152H

Open Access Article. Published on 16 Dezember 2025. Downloaded on 04.04.2026 08:28:47.
This article is licensed under a Creative Commons Attribution 3.0 Unported Licence.

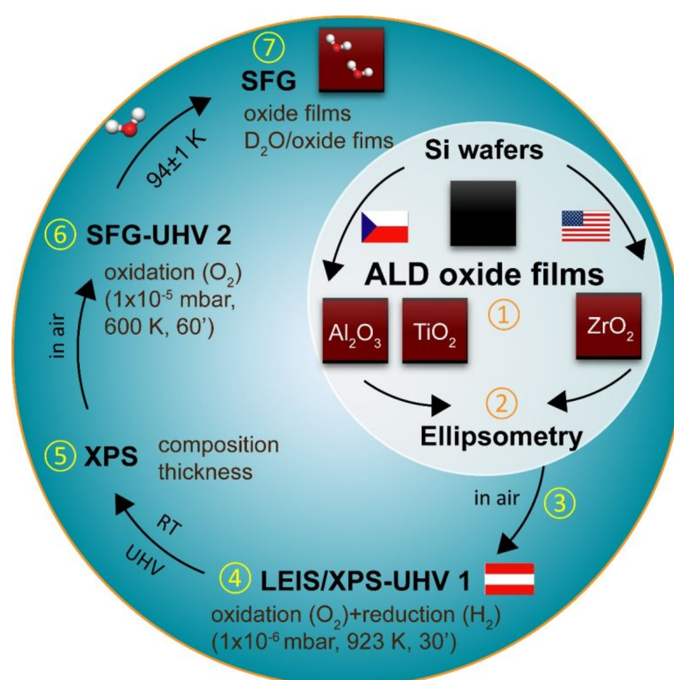

Figure 1 Schematic diagram of the ALD-sample preparation and characterization process.

Characterization of ALD oxide films by XPS and SFG

XPS

The oxide film thicknesses were measured by ellipsometry, yielding about 5.1 nm for Al_2O_3, 5.0 nm for TiO_2, and 6.9 nm for ZrO_2. However, in this thickness range, ellipsometry is neither as accurate as XPS, nor does it provide compositional information.

When exposed to air at room temperature, Si wafers naturally form a passivating SiO_2 layer (i.e., native (n-)SiO_2; depending on exposure time and humidity), typically ranging from a few angstroms (Å) to several nanometers (nm)[44-46]. Accordingly, the ALD films were deposited on top of these n-SiO_2 layers (in our case, ~2.3 nm by ellipsometry).

Faraday Discussions Accepted Manuscript

The Si wafer substrate is best represented by the XPS Si 2p region, whereas the individual ALD films were characterized by the Al 2p, Zr 3d, and Ti 2p regions (**Figure S1**). The binding energy positions and line shapes of Al 2p, Zr 3d and Ti 2p region spectra correspond well to literature values[47-49] for Al_2O_3, TiO_2, and ZrO_2, respectively. Detailed fitting procedures are provided in the **Supplementary Materials**. The film thicknesses of the ALD oxides as well as of the SiO_x/n-SiO_2 interlayers were calculated from the mentioned region spectra applying a multilayer electron attenuation model based on the Strohmeier approach[50]. The corresponding results are summarized in

View Article Online
DOI: 10.1039/D5FD00152H

Table 1.

Table 1 Binding energies and film thicknesses of all oxide films grown on Si wafer.

Samples	Al_2O_3/SiO_x/n-SiO_2		ZrO_2/n-SiO_2		TiO_2/n-SiO_2	
	Al 2p	Si 2p	Zr 3d	Si 2p	Ti 2p	Si 2p
BE (eV)	74.1	99.3/101.8	181.9	102.2	458.9	102.2
Oxide film	Al_2O_3	SiO_x/SiO_2	ZrO_2	SiO_2	TiO_2	SiO_2
Thickness (nm)	4.9	≈1.1	4.3	1.1	4.3	1.1
Sum (nm)	6.0		5.4		5.4	

Ti and Zr have comparably high oxygen affinities (due to similar enthalpies of oxide formation) but react with SiO_2 only at elevated temperatures (> 900 K)[51, 52]. As a result, the original n-SiO_2 layer (1.1 nm) was largely preserved during ALD growth of TiO_2 and ZrO_2, producing a consistent Si 2p peak at 102.2 eV and an n-SiO_2 thicknesses of 1.1 nm in both cases. In contrast, Al has an even higher oxygen affinity, enabling partial reduction of the n-SiO_2 and formation of Si suboxides ("SiO_x", 99.3 eV). This caused a downward binding energy shift of the Si 2p region by 0.4 eV. Since nothing further can be said about the crystallography of SiO_x, it is assumed as first approximation that the reduction of n-SiO_2 has not significantly changed the thickness of the passivation layer (≈1.1 nm). Below, the n-SiO_2 surface is simply referred to as "Si wafer".

SFG: 2150-3000 cm^{-1}

After the XPS measurements, the samples were transferred to the SFG cell for further characterization. The SFG spectra can be measured using the ssp or ppp polarization combinations[19-22]. Here, s and p denote polarizations of the optical field perpendicular to and within the plane of incidence, respectively. They are listed in the order of relative beam energies (for example, s-SFG, s-visible and p-IR). Prior to SFG, all oxide films were pretreated to remove carbonaceous and/or hydrocarbon (organic) contaminants. As shown in **Figure S2**, the C-H stretching peaks at 2800-3000 cm^{-1} decreased

Open Access Article. Published on 16 Dezember 2025. Downloaded on 04.04.2026 08:28:47.
This article is licensed under a Creative Commons Attribution 3.0 Unported Licence.

Faraday Discussions Accepted Manuscript

View Article Online
DOI: 10.1039/D5FD00152H

significantly after annealing in O_2 (1x10^{-5} mbar O_2, 600 K, 60 min) compared with annealing under UHV conditions. Therefore, for all subsequent SFG measurements, the oxide films were routinely pretreated by oxidation.

We then measured the SFG spectra of the oxide films in the range of 2100-2800 cm^{-1} (**Figure 2**), which includes the O-D stretching region (used as a reference for the D_2O spectra) and C-H stretching region[53] (used to evaluate residual organic contaminants) at 100/140 K. An SFG spectrum of the Si wafer at 295 K was also measured for reference. The non-resonant SFG responses from the Si wafer with an intrinsic ~ 2.3 nm SiO_2 passivation layer (black), as well as from the Si-supported Al_2O_3 (blue), ZrO_2, (red) and TiO_2 (green) films, were essentially identical. This indicates that all the metal oxide films (4.3-4.9 nm) produced no detectable non-resonant SFG signal, which is further supported by the distinctly different SFG response observed for a 60 nm TiO_2 film[54].

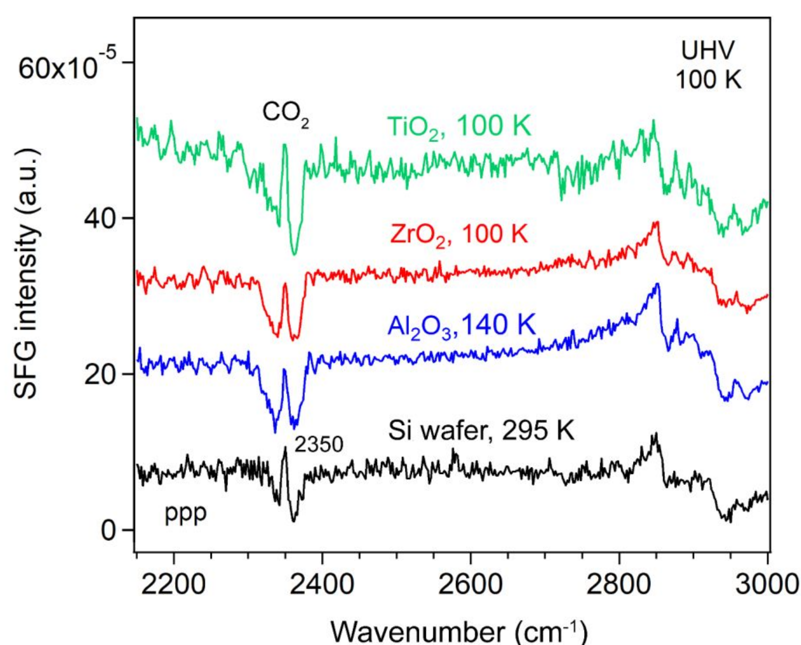

Figure 2 ppp-SFG spectra of Si wafer and ~5-nm ALD films of Al_2O_3, ZrO_2, and TiO_2 at 100 K under UHV, with offset for clarity.

SFG: 3000-3800 cm^{-1}

We also measured the SFG spectra of neat Si wafer and Si-supported oxide films under UHV in the O-H stretching region (3000-3800 cm^{-1}) at 100 K. Interestingly, a peak at 3720 cm^{-1} was observed (**Figure 3**), which is attributed to the dangling O-H bonds pointing out of the ice at the surface, i.e., the "free" O-H stretching mode, arising from trace water molecules present in the UHV chamber. The signal originates from the total population of water molecules in the DAA, DA, and AA configurations that exhibit "free" O–H groups[40]. This "free" O-H peak disappeared upon heating to room temperature (**Figure S3**).

Open Access Article. Published on 16 Dezember 2025. Downloaded on 04.04.2026 08:28:47.
This article is licensed under a Creative Commons Attribution 3.0 Unported Licence.

Faraday Discussions Accepted Manuscript

View Article Online
DOI: 10.1039/D5FD00152H

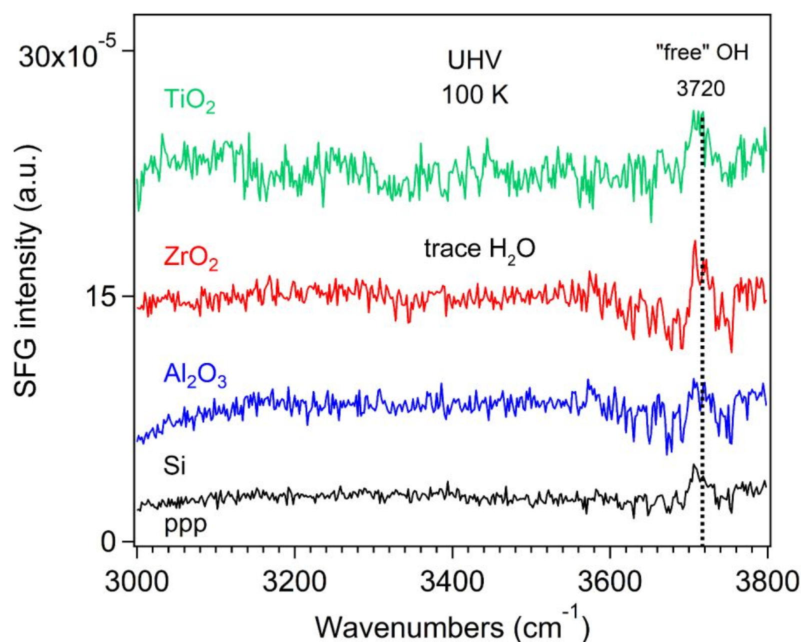

Figure 3 ppp-SFG spectra of oxide films at 100 K under UHV in the range of 3000-3800 cm^{-1}.

Open Access Article. Published on 16 Dezember 2025. Downloaded on 04.04.2026 08:28:47.
This article is licensed under a Creative Commons Attribution 3.0 Unported Licence.

Faraday Discussions Accepted Manuscript

Nagata and coworkers[40] reported that the topmost monolayer of water on the basal face of ice (from 150 K to 245 K) exhibits a minimum number of "free" O-H groups and a maximum in hydrogen bonding around 200 K. Above 200 K, thermal fluctuations break hydrogen (H) bonds and generate more free O-H groups; below 200 K, the formation of bulk-like crystalline interfacial structures also results in H-bond breaking, thereby increasing the population of free O-H groups. At 300 K, H_2O (D_2O) was reported to be partially dissociated on the Si(111) surface to form the SiOH (SiOD) species[55]. As the monolayer water desorption occurs at around 171 K and gradually moves to low temperature (150 K) with increasing the water thicknesss[39]. Shen and coworkers[37] found that the "free" OH band in both ssp and ppp polarization combinations becomes narrower with decreasing temperature (170-270 K), which they attributed to a narrowing of the orientational distribution of O-H bond. Below 200 K, the "free" OH groups align almost perfectly upright with an assumption of a truncated flat distribution, indicating the absence of a quasi-liquid layer (QLL) or any surface layer with significant fluidity. Above 200 K, the onset and evolution of QLL introduce surface disorder[37].

SFG spectra of D_2O ice on a Si substrate and Si-supported oxide films in the O-D stretching region (2150-2800 cm^{-1})

Low D_2O exposure

We initially measured SFG spectra of D_2O adsorption at room temperature, but no signal was detected due to desorption[39]. Consequently, we focused on spectra acquired at low temperature 94 ± 1 K, the minimum achievable with liquid N_2 cooling.

View Article Online
DOI: 10.1039/D5FD00152H

At the liquid D_2O-air interface[34], three characteristic peaks appeared at 2390 (broad), 2520 (broad), and ~2725 cm^{-1}, corresponding to strongly H-bonded OD, weakly H-bonded OD, and dangling OD groups, respectively. **Figure 4** compares the ppp-SFG spectra of D_2O adsorbed on a Si substate and on Si-supported Al_2O_3, ZrO_2, and TiO_2 films at 93-95 K under low D_2O exposure. It has been reported that dosing 5 L of D_2O at 90 K initially forms an amorphous ice multilayer; upon heating 160 K, an ordered monolayer is formed which remains stable up to 210 K[56]. Therefore, the spectra shown in **Figure 4** originate from multilayer ice**.** For reference, the ice growth rate on Pt(111) has been reported to be 0.03 monolayers (ML) per second at a water pressure of 5×10^{-8} Torr[39]. Herein, we assumed that 1 L of ice corresponds to a water flux of 10^{-6} mbar·s.

Five distinct features were observed in **Figure 4**, centered at approximately 2310, 2350, 2450, 2650 and 2730 cm^{-1}. These bands are assigned to strongly hydrogen-bonded OD stretching of highly ordered water (D_2O) molecules in ice I_h crystal (D_2O-D_2O H-bonded OD_1), CO_2 gas adsorption (originating from residual CO_2 in the lab atmosphere beam path), weakly H-bonded O-D stretching of less-ordered D_2O molecules (D_2O-D_2O H-bonded OD_2), weakly H-bonded OD stretching of D_2O interacting with the oxide film (D_2O-oxide H-bonded OD_3), and the "free" OD stretching of the topmost D_2O molecules, respectively. The D_2O-D_2O H-bonds may arise from both interlayer and intralayer water molecules[41]. A peak near 2730 cm^{-1} corresponding to "free" OD groups has also been reported for intact water molecules weakly bound on the terrace sites of Mn_3O_4(111)[57].

On the Al_2O_3 surface under low exposure conditions, the absence of the H-bonded OD_1 feature indicates that the surface is initially populated primarily by water species with a "free" (non-hydrogen-bonded) OD group, alongside water species exhibiting weak water-water and water-oxide interaction. This suggests that strong interlayer and intralayer molecular interactions among water molecules are established only at higher coverages. Consequently, we performed additional measurements at varying D_2O exposures at 93-95 K.

Open Access Article. Published on 16 Dezember 2025. Downloaded on 04.04.2026 08:28:47.
This article is licensed under a Creative Commons Attribution 3.0 Unported Licence.

Faraday Discussions Accepted Manuscript

View Article Online
DOI: 10.1039/D5FD00152H

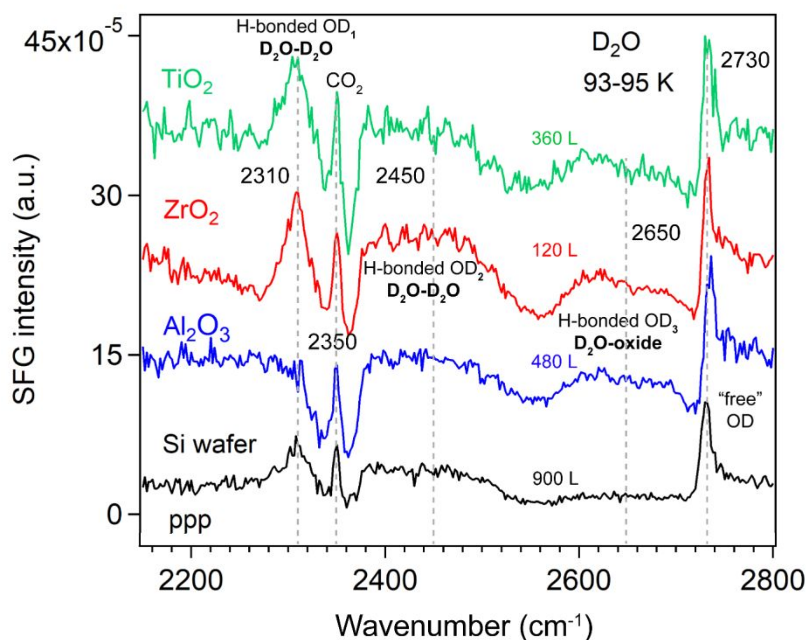

Figure 4 ppp-SFG spectra of D_2O adsorption on Si wafer, Si-supported ~5-nm ALD films of Al_2O_3, ZrO_2, and TiO_2 at 93-95 K at relatively low D_2O exposures (below 900 L). D_2O exposure conditions are as follows: Si wafer, 5 x 10^{-6} mbar for 180 s; Al_2O_3, 4 x 10^{-7} mbar for 1200 s; ZrO_2, 2 x 10^{-7} mbar for 600 s; and TiO_2, 2 x 10^{-7} mbar for 1800 s.

Open Access Article. Published on 16 Dezember 2025. Downloaded on 04.04.2026 08:28:47.
This article is licensed under a Creative Commons Attribution 3.0 Unported Licence.

Faraday Discussions Accepted Manuscript

Variation of D_2O exposures

Si wafer

The H-bonded OD_3 band (~2650 cm^{-1}) in **Figure 4**, assigned to H-bonds between water and the oxide film, is observed on all oxide films (Al_2O_3, ZrO_2, and TiO_2). For D_2O (10 layers) adsorption on 0.5 ML CO/Pt(111) at 140 K, four O–D features have been reported: two broad bands at 2278 and 2472 cm^{-1} assigned to hydrogen-bonded OD symmetric and asymmetric stretching modes, respectively, and two weaker bands at 2675 and 2720 cm^{-1} corresponding to O–D stretching of D_2O interacting with CO at the D_2O/CO interface and the "free" OD at the vacuum/ice interface[58]. The peak at 2675 cm^{-1} is qualitatively like the OD_3 feature observed in **Figure 4.**

This assignment is supported by its absence on the Si substrate. However, it is also possible that the signal on Si is simply too weak to detect. Furthermore, because a D_2O molecule contains two OD groups, one can act as "free" OD (at ~3730 cm^{-1}) pointing toward the vapor phase, while the other points toward the oxide surface. The latter OD group may form H-bonds either with the oxide film or with neighboring water molecules. For example, at the liquid-air interface, a broad peak at 3550 cm^{-1} has been attributed to the H-bonded O-H stretching mode with $C_{\infty v}$ symmetry, arising from water molecules with one "free" and one H-bonded OH group[59]. If the OD group responsible for the OD_3 band were primarily H-bonded to neighboring water molecules, then this feature should also appear

View Article Online
DOI: 10.1039/D5FD00152H

on the Si surface. To rule out these possibilities, we measured the SFG spectra of D_2O adsorption on the Si substrate as a function of D_2O exposure—controlled by adjusting the D_2O vapor pressure and/or the exposure time—corresponding to progressively thicker ice layers.

However, the exposure-dependence of SFG spectra clearly rules out such possibilities. As shown in **Figure 5**, no signal appears in the 2600-2700 cm^{-1} region. Therefore, the OD_3 stretching mode in **Figure 4** most probably originates from hydrogen bonding interactions involving water molecules (e.g., DAA, DA) with one "free" OD group or from species (e.g., DDA) in which both OD groups are bonded directly to the oxide surface. This band cannot be assigned to dissociated O–H species, as the stretching frequency of dissociated O–H groups is much higher than that of free O–H in molecularly adsorbed D_2O[60].

Additionally, as D_2O exposure increases on Si wafer, the intensity of the "free" OD signal decreases, while the weakly H-bonded OD_2 and strongly H-bonded OD_1 peaks increase. The weak OD_2 peak, however, remains several times weaker than the strong OD_1 peak.

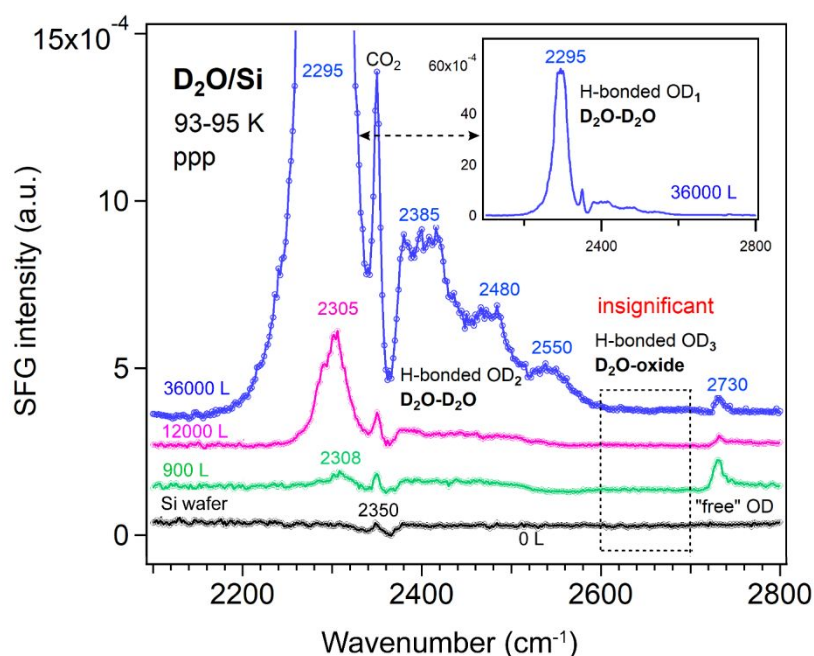

Figure 5 ppp-SFG spectra of D_2O adsorbed on a Si wafer with increasing D_2O exposure at 93-95 K. The insert shows the full-scale spectrum obtained after exposure to $3x10^{-4}$ mbar D_2O for 2 min at 93-95 K. D_2O exposure conditions are as follows: black, no; green, 5 x 10^{-6} mbar for 180 s; pink, 1 x 10^{-4} mbar for 120 s; and blue, 3 x 10^{-4} mbar for 120 s.

Similarly, D_2O adsorption on the Al_2O_3, ZrO_2, and TiO_2 ALD films at 93-95 K was systematically investigated as a function of D_2O exposure. All SFG spectra were recorded in the 2150-2800 cm^{-1} range. To clearly illustrate the spectral evolution, the spectra corresponding to the H-bonded OD_2, H-bonded OD_3, and "free" OD modes are presented separately, each with an appropriately scaled y-axis.

Open Access Article. Published on 16 Dezember 2025. Downloaded on 04.04.2026 08:28:47.
This article is licensed under a Creative Commons Attribution 3.0 Unported Licence.

Faraday Discussions Accepted Manuscript

View Article Online
DOI: 10.1039/D5FD00152H

Al_2O_3 film

Figure 6 shows the ppp-SFG spectra of D_2O adsorption on the Al_2O_3 film. The five peaks (also shown in **Figure 4**) vary differently with increasing ice layer thickness. As the D_2O exposure increases, the OD_1 stretching band shifts to lower wavenumbers (from 2308 to 2283 cm^{-1}) and increases in intensity (**Figure 6a**). This behavior can be attributed not only to stronger intermolecular interactions among water molecules but also to an increased population of molecules adopting an ordered structure. On Pt(111) single crystal surfaces, the strong enhancement of the O-H stretching resonance with increasing ice thickness arises from surface-induced polar ordering, generated by polar anchoring of the first ice monolayer on Pt[39].

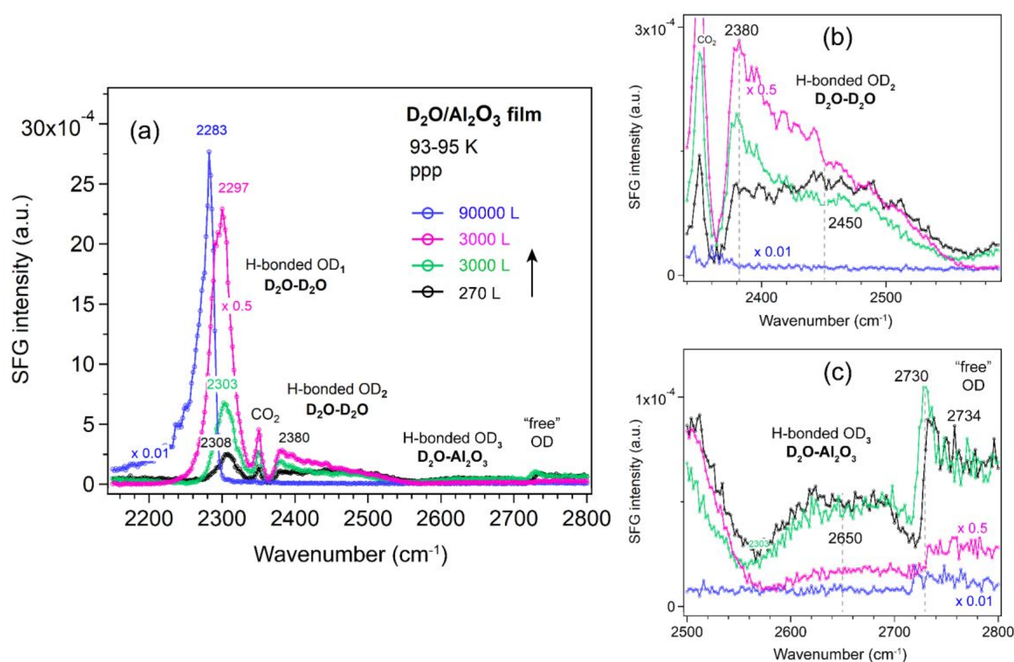

Figure 6 (a) ppp-SFG spectra in the O-D stretching region of D_2O adsorbed on an ALD-grown Al_2O_3 film on Si wafer with increasing D_2O exposure at 93-95 K. For clarity, ppp spectra with appropriately adjusted y-axis scales are shown in (b) for the OD_2 region (2340-2580 cm^{-1}) and in (c) for the OD_3 and "free" OH regions (2500-2800 cm^{-1}). D_2O exposure conditions are as follows: black, 1.5 x 10^{-6} mbar for 180 s; green, 5 x 10^{-5} mbar for 60 s; pink, 1 x 10^{-4} mbar for 30 s; and blue, 2.5 x 10^{-5} mbar for 3600 s.

In contrast, the weakly bonded OD_2 stretching band (**Figure 6b**) initially increases and then decreases in intensity. At low exposure (black curve), the OD_2 band is broad (2450 cm^{-1}), but it becomes narrower and shifts to lower wavenumbers (2380 cm^{-1}) as the exposure increases (green and pink curves).

The weakly H-bonded OD_3 stretching and "free" OD bands show trends similar to OD_2, but they vanish at earlier stages—disappearing at an exposure of 1x10^{-4} mbar for 30 s (**Figure 6c**). These observations are further supported by the SFG spectra collected using the *ssp* polarization combination (**Figure 7a-c**). According to the SFG selection rules[61], since at 270 L the OD_2 peak at 2450 cm^{-1} is stronger in the ppp spectrum (**Figure 6b**) than in the ssp (**Figure 7b**) spectrum, whereas the 2380 cm^{-1} peak is stronger

Open Access Article. Published on 16 Dezember 2025. Downloaded on 04.04.2026 08:28:47.
This article is licensed under a Creative Commons Attribution 3.0 Unported Licence.

Faraday Discussions Accepted Manuscript

View Article Online
DOI: 10.1039/D5FD00152H

in ssp (**Figure 7b**) than in ppp (**Figure 6b**), the former can be assigned to the O-D asymmetric stretch, and the latter to the symmetric stretch of weakly bonded water. When the surface is exposed to 2.5x10^{-5} mbar D_2O for one hour (blue curve), the OD_1 signal increases several times, while all other bands disappear completely.

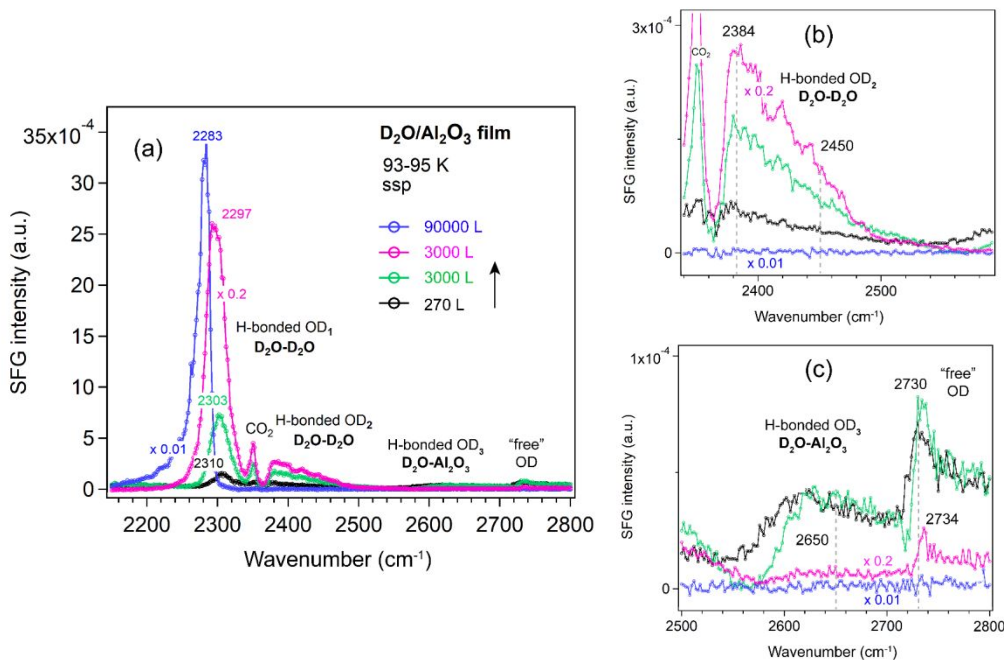

Figure 7 (a) ssp-SFG spectra in the O-D stretching region of D_2O adsorbed on an ALD-grown Al_2O_3 film on Si wafer with increasing D_2O exposure at 93-95 K. For clarity, ssp spectra with appropriately adjusted y-axis scales are shown in (b) for the OD_2 region (2340-2580 cm^{-1}) and in (c) for the OD_3 and "free" OH regions (2500-2800 cm^{-1}). D_2O exposure conditions are as follows: black, 1.5 x 10^{-6} mbar for 180 s; green, 5 x 10^{-5} mbar for 60 s; pink, 1 x 10^{-4} mbar for 30 s; and blue, 2.5 x 10^{-5} mbar for 3600 s.

Open Access Article. Published on 16 Dezember 2025. Downloaded on 04.04.2026 08:28:47.
This article is licensed under a Creative Commons Attribution 3.0 Unported Licence.

The hydrogen-bond network in D_2O can be viewed *analogously* to that in H_2O. ppp-SFG studies of H_2O-ice (-17 °C) and liquid water (23°C) adjacent to a sapphire (Al_2O_3) prism have been reported[31]. Compared with liquid water, the strongly H-boned O-H peak is red-shifted from ~3200 to ~3150 cm^{-1} in ice, indicating stronger intermolecular hydrogen bonding. In contrast, the "free" O-H mode is blue-shifted from ~3700 to ~3740 cm^{-1} and decreases in intensity. Notably, no distinct weakly bonded O-H features associated with H_2O-H_2O and H_2O-Al_2O_3 interactions were observed[31]. The absence of these signals is probably due to the reduced structural ordering of water molecules at 256 K compared with the highly ordered structure at 95 K (**Figure 6**).

The strongest peak at 3098 cm^{-1}, assigned to water molecules forming bilayer-stitching hydrogen bonds, contained a substantial quadrupole bulk contribution that produces a 90° phase shift relative to a purely interfacial mode[62]. A new O-H stretching band of H_2O-ice at 3530 cm^{-1} has been observed by heterodyne-detected (HD)-SFG and arises from a combination of the asymmetric O-H stretch of

Faraday Discussions Accepted Manuscript

fully coordinated DDAA molecules and the symmetric O-H stretch of DDA water molecules with opposite phase[62].

View Article Online
DOI: 10.1039/D5FD00152H

MD and *ab initio* studies revealed that the structural influence of graphene on water is extremely local: strong ordering is observed only in the first water layer, while subsequent layers exhibit bulk-like behavior. Stratification does not persist beyond ~ 5 Å from the graphene surface[63]. Thus, at high water exposures (**Figure 6** and **Figure 7**), the SFG signal primarily reflects the ice-vapor interface rather than the ice-oxide interface, consistent with the disappearance of the OD_3 peak (associated with hydrogen bonds between water and the oxide film).

For ice on metal single crystal surfaces, the behavior is different. On Pt(111)[39], as the ice film thickness increased from 1.2 to 26.4 ML, the H-bonded O–H peak (~3100 cm^{-1}) intensifies were dramatically enhanced and red-shifted, in contrast to the blue-shift behavior observed in **Figure 6**.

The $Im\chi^{(2)}$ SFG spectrum of the H-bonded O-H (or O-D) stretching region of H_2O (D_2O) ice film exhibits multiple peaks with exclusively negative, indicating net-H-down (or net-D-down) ferroelectric orientational ordering in which protons (or deuterons) preferentially point toward the Pt substrate[64]. The orientation of the interfacial water plays a key role in ice structure: freezing water next to a positively charged sapphire surface yields a stronger ice signal than liquid water, whereas freezing near a negatively charged mica surface produces proton-disordered ice, causing strong attenuation of the SFG signal[65].

Because the ssp spectra of the D_2O on Al_2O_3 film (**Figure 7**) showed no additional features or significant enhancements compared to the ppp spectra (**Figure 6**), all spectra of the other oxides (ZrO_2, TiO_2, and CoO) were measured only in the ppp polarization combination.

Open Access Article. Published on 16 Dezember 2025. Downloaded on 04.04.2026 08:28:47.
This article is licensed under a Creative Commons Attribution 3.0 Unported Licence.

ZrO_2 film

Similar trends as for Al_2O_3 were observed for the ZrO_2 film (**Figure 8**). The OD_1 band increased in intensity and shifted to lower wavenumbers (from 2310 to 2293 cm^{-1}). Because the surface was not exposed to a sufficiently large amount of water, the disappearance of the OD_1 band was not observed. However, overall decreases in the OD_3 and “free” OD bands were observed with increasing D_2O exposure, consistent with the behavior seen on the Si (**Figure 5**) and Al_2O_3 (**Figure 6**) surfaces.

Faraday Discussions Accepted Manuscript

View Article Online
DOI: 10.1039/D5FD00152H

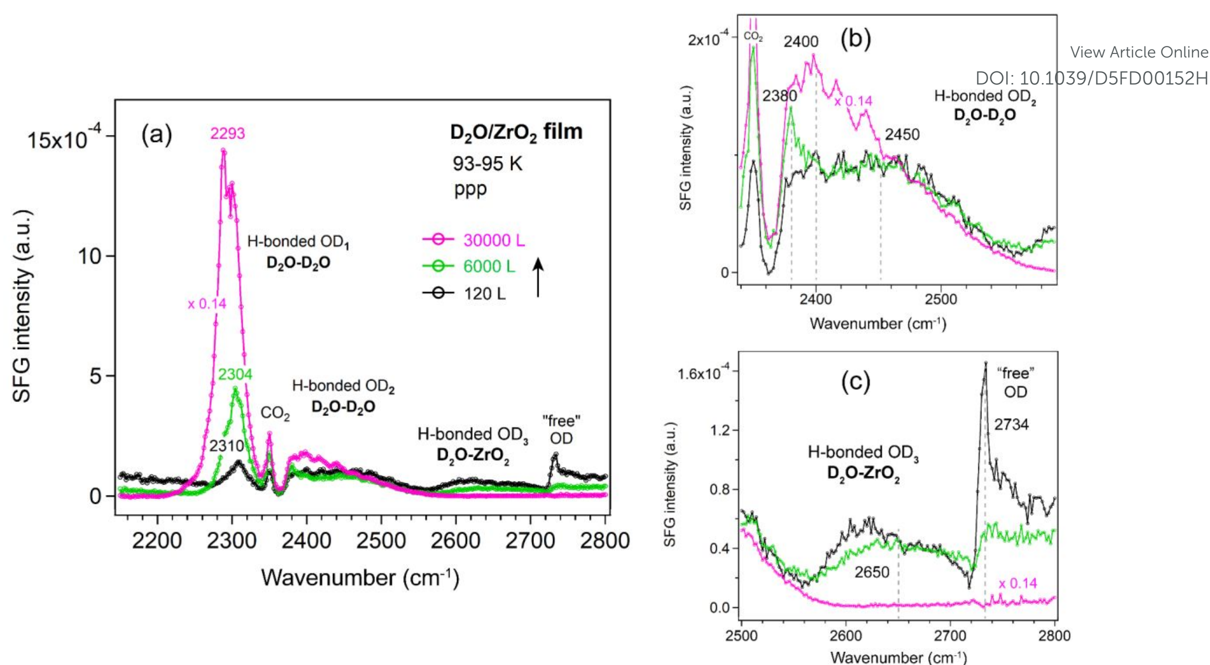

Figure 8 (a) ppp-SFG spectra in the O-D stretching region of D_2O adsorbed on an ALD-grown ZrO_2 film on Si wafer with increasing D_2O exposure at 93-95 K. For clarity, ppp spectra with appropriately adjusted y-axis scales are shown for (b) the OD_2 region (2340-2580 cm^{-1}) and (c) the OD_3 and "free" OH regions (2500-2800 cm^{-1}). D_2O exposure conditions are as follows: black, 2 x 10^{-7} mbar for 600 s; green, 1 x 10^{-5} mbar for 600 s; and pink, 5 x 10^{-5} mbar for 600 s.

TiO_2 film

For TiO_2 films (**Figure 9**), the OD_1 band initially behaves similarly to that on Al_2O_3 and ZrO_2, showing an increase in intensity and a shift from 2310 to 2293 cm^{-1} at low D_2O exposure. At higher exposure (1 × 10^{-4} mbar), prolonged dosing leads to a decrease in intensity and a pronounced shift to lower wavenumbers (2265–2230 cm^{-1}). This behavior is consistent with earlier reports that the crystallization rate of amorphous solid water decreases sharply with increasing film thickness, likely to be crystallization-induced cracking[66]. The observed OD_1 decrease on TiO_2 is therefore attributed to film cracking under high water vapor pressures. When the sample is cooled from the bottom using liquid N_2, crystallization of the thin film proceeds more slowly than ice sublimation. In addition, SFG studies of D_2O at the solid-liquid interface of TiO_2 films with thickness of 85 and 150 nm have been reported[67]; however, no peak was observed in the 2600-2700 cm^{-1} region.

Open Access Article. Published on 16 Dezember 2025. Downloaded on 04.04.2026 08:28:47.
This article is licensed under a Creative Commons Attribution 3.0 Unported Licence.

Faraday Discussions Accepted Manuscript

View Article Online
DOI: 10.1039/D5FD00152H

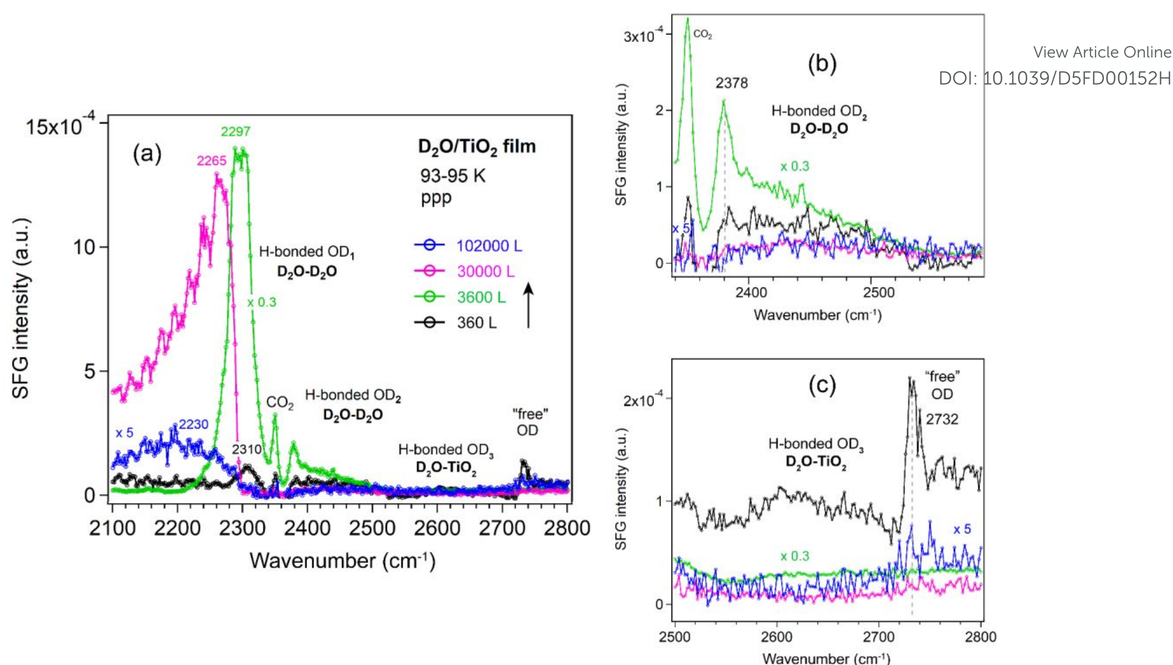

Figure 9 (a) ppp-SFG spectra in the O-D stretching region of D_2O adsorbed on an ALD-grown TiO_2 film on Si wafer with increasing D_2O exposure at 93-95 K. For clarity, ppp spectra with appropriately adjusted y-axis scales are shown for (b) the OD_2 region (2340-2580 cm^{-1}) and (c) the OD_3 and "free" OH regions (2500-2800 cm^{-1}). D_2O exposure conditions are as follows: black, 2 x 10^{-7} mbar for 1800 s; green, 1 x 10^{-5} mbar for 360 s; pink, 1 x 10^{-4} mbar for 300 s; and blue, 1 x 10^{-4} mbar for 1020 s.

It was reported that the variation in the H_2O-metal binding energy varies little from metal to metal[28]. As Al_2O_3 and ZrO_2 films were only exposed to relatively lower vapor pressures (< 1x10^{-4} mbar), a similar decrease in the OD_1 band would also be expected if they were exposed to higher vapor pressures for longer durations. Therefore, there is no significant difference in the overall water structure among the Al_2O_3, ZrO_2, and TiO_2 films.

CoO film

To complement our observations on the three ALD-grown films, we also measured the SFG spectra of D_2O adsorption on a CoO film under similar conditions (**Figure 10**). The CoO was prepared by oxidizing an unpolished Co foil in 10^{-6} mbar O_2 at 873 K for 5 h (similar to ref[68]) . The subsequent LEIS spectrum (**Figure S4**) showed two features assigned solely to Co and O surface species based on a LEIS calculator[69]. The low background intensity below 500 eV further confirmed a clean surface without impurities such as carbon[70]. XPS analysis of the Co 2p region (**Figure S5**) revealed no metallic Co signals and showed features characteristic of CoO, consistent with the work of Biesinger et al.[71] Deconvolution of the Co 2p spectrum showed two contributions associated with Co^{2+} at 779.9 eV and 782.1 eV (Co $2p_{3/2}$), accompanied by two shake-up satellites and a spin-orbit splitting of 15.9 eV (**Figure S5**), in agreement with literature[71-73]. In the O 1s region (**Figure S6**), the main peak at 529.8 eV was

Open Access Article. Published on 16 Dezember 2025. Downloaded on 04.04.2026 08:28:47.
This article is licensed under a Creative Commons Attribution 3.0 Unported Licence.

Faraday Discussions Accepted Manuscript

assigned to lattice oxygen in CoO, while a weak shoulder at around 531.1 eV was attributed to adsorbed oxygen species such as OH groups[71, 73, 74]. Furthermore, the Co:O stoichiometry determined from the relative XPS peak intensities was approximately 1:1, confirming the formation of a CoO film on the Co foil.

View Article Online
DOI: 10.1039/D5FD00152H

The CoO film was then transferred in air for SFG measurements. To remove potential contaminants introduced during air exposure, the CoO film was oxidized in 1x10^{-6} mbar O_2 at 573 K for 60 min, following a similar procedure used for the ALD-grown oxides. After pretreatment, the spectrum of the CoO film was very similar to that of a Si-wafer (**Figure S7**) and the ALD-grown oxide films (**Figure 2**), indicating that no significant differences in the non-resonant SFG signals.

After growing ice on the CoO film, the OD_1, OD_2 and "free" OD bands (**Figure 10**) exhibited trends similar to those observed on Al_2O_3 and ZrO_2 films. Because the Co foil was unpolished, the resulting CoO film was grown on a substrate with sub-micrometer roughness (**Figure S8**). Consequently, due to strong signal scattering from the rough surface, the "free" OD peak was at least 5 times weaker than on the flat ALD-grown films, and the OD_3 band (water-oxide) could not be detected. Furthermore, even after exposure to 5x10^{-4} mbar D_2O for 30 min, no decrease in the OD_1 band (2284 cm^{-1}) is observed, in contrast to the TiO_2 film, where the OD_1 band shifts to 2230 cm^{-1} at 1x10^{-4} mbar after 17 min. Given the > 50 cm^{-1} red shift of the OD_1 band on TiO_2, these results clearly indicate that the water structure on the TiO_2 film, especially at higher vapor pressures, behaves differently from that on Al_2O_3, ZrO_2, and CoO films, regardless of whether the oxide is ALD-grown or formed by direct oxidation of a metal foil. For completeness we mention that roughness on the nanometer-scale may enhance SFG signals, such as that of CO adsorbed on rough Ir surfaces (created by ion-sputtering), as compared to smooth Ir(111)[75]. The enhancement is attributed to localized surface plasmon resonances (LSPR). Similarly, CO on 45 nm Pt nanoparticles yielded much stronger signal than on smooth Pt films[76].

Open Access Article. Published on 16 Dezember 2025. Downloaded on 04.04.2026 08:28:47.
This article is licensed under a Creative Commons Attribution 3.0 Unported Licence.

Faraday Discussions Accepted Manuscript

View Article Online
DOI: 10.1039/D5FD00152H

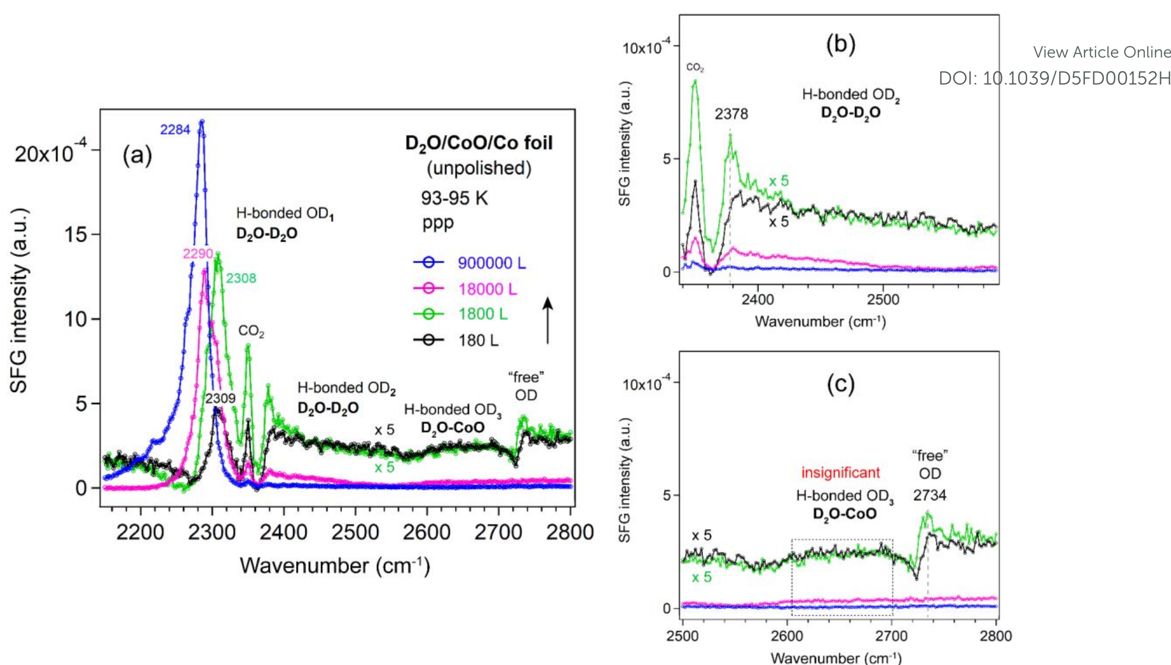

Figure 10 (a) ppp-SFG spectra in the O-D stretching region of D_2O adsorbed on CoO film/unpolished Co foil with increasing D_2O exposure at 93-95 K. For clarity, ppp spectra with appropriately adjusted y-axis scales are shown in (b) for the OD_2 region (2340-2580 cm^{-1}) and in (c) for the OD_3 and "free" OH regions (2500-2800 cm^{-1}). D_2O exposure conditions are as follows: black, 1 x 10^{-6} mbar for 180 s; green, 1 x 10^{-5} mbar for 180 s; pink, 1 x 10^{-4} mbar for 180 s; and blue, 5 x 10^{-4} mbar for 1800 s.

SFG spectra of D_2O ice adsorbed on a Si substrate and three oxide films in the O-H stretching region (3000-3800 cm^{-1})

Under ambient conditions, most metal oxide surfaces are decorated with hydroxyl groups, a consequence of water dissociative chemisorption[77]. The SFG signal from surface hydroxyl groups can be quenched by the addition of methanol[78]. When exposed to an aqueous environment, pristine minerals such as SiO_2[79], Al_2O_3[80], and TiO_2[81] can hydroxylate to form terminal hydroxyl (-OH) groups. However, our results showed that no OH groups were detectable at room temperature (295 K) (**Figure 11**).

After dosing with high-pressure D_2O, a weak and broad hydrogen bonded O-H stretching band[82] centered at 3300 cm^{-1} was observed on all ALD-grown oxide films, likely to be trace H_2O introduced to the chamber via the gas line. This peak shifted to 3270 cm^{-1} on the Si substrate at higher D_2O exposure. Furthermore, a similar red shift from the hydrogen-bonded O-H band to the OD_1 band was observed, accompanied by the disappearance of the "free" OH signal. These findings are consistent with **Figure 6**-**Figure 10** and agree with previous studies reporting that at 80 K, no free OH bond was present in the H-down bilayer structure[79]. In addition, the relatively weak H-bonded OH and "free" OH signals in **Figure 11** were not observed on the rough CoO/Co foil surfaces (**Figure S9**), also due to signal scattering from rough surfaces.

Open Access Article. Published on 16 Dezember 2025. Downloaded on 04.04.2026 08:28:47.
This article is licensed under a Creative Commons Attribution 3.0 Unported Licence.

Faraday Discussions Accepted Manuscript

View Article Online
DOI: 10.1039/D5FD00152H

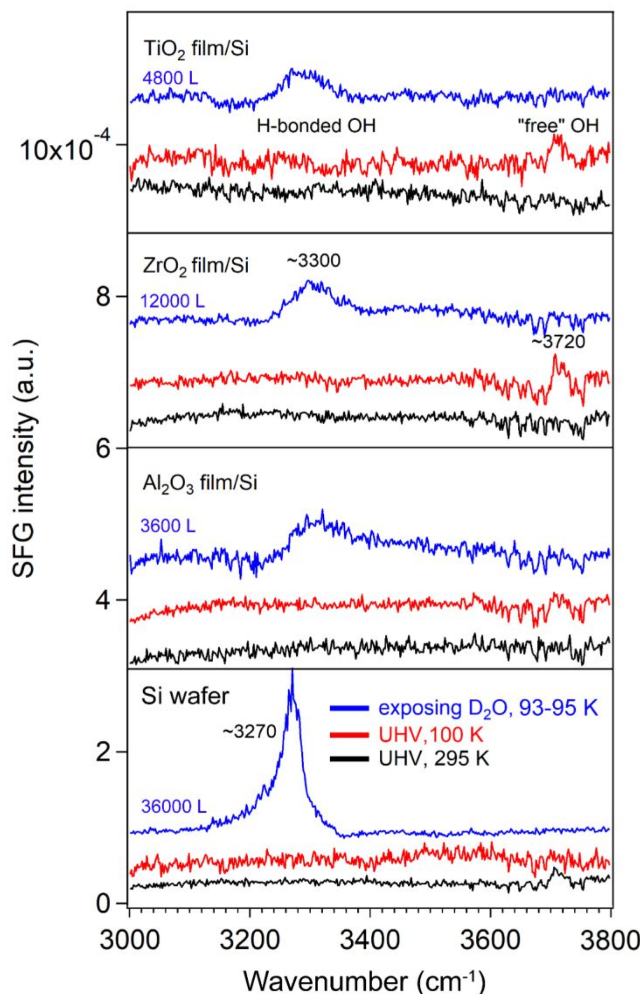

Open Access Article. Published on 16 Dezember 2025. Downloaded on 04.04.2026 08:28:47.
This article is licensed under a Creative Commons Attribution 3.0 Unported Licence.

Faraday Discussions Accepted Manuscript

Figure 11 ppp-SFG spectra in the O-H stretching region for bare Si substrate and ALD-films of Al_2O_3, ZrO_2, and TiO_2 surfaces. D_2O exposure conditions are as follows: bare Si, 3 x 10^{-4} mbar for 120 s; Al_2O_3 film/Si, 2 x 10^{-6} mbar for 1800 s; ZrO_2 film/Si, 2 x 10^{-5} mbar for 600 s; and TiO_2 film/Si, 1 x 10^{-5} mbar for 480 s.

Conclusions and outlook

SFG spectra of D_2O adsorption (ice formation) on ALD-grown Al_2O_3, ZrO_2, and TiO_2 films at 93-95 K have been investigated. It was revealed that the interaction between ice and the oxide surfaces was relatively weak, primarily exhibiting a broad O-D stretching feature near 2650 cm^{-1} (OD_3 band), with minimal dependence on oxide composition. This feature was observed for the first time and remained detectable up to exposures of 3 000 L on Al_2O_3, 6000 L on ZrO_2, and 360 L on TiO_2. In contrast, it was not observable on the CoO film supported on a rough Co foil because the signal was too weak, probably due to signal scattering. Upon further increase in D_2O exposure (>10^4 L), spectral contributions from the ice-oxide interface were progressively overshadowed by those from the ice-vapor interface (OD_1 and OD_2 bands). At sufficiently high exposures, the disappearance of the “free” O-D stretch indicated that all interfacial molecules became hydrogen-bonded, consistent with the formation of an H-down bilayer structure[79].

View Article Online
DOI: 10.1039/D5FD00152H

At the ice-vapor interface (≥30,000 L), among the oxides studied, TiO_2 exhibits notably distinct behavior: the strongly hydrogen-bonded OD_1 mode undergoes an anomalous red-shift to 2230 cm^{-1} accompanied by significant intensity loss, indicating the formation of unique water structures on this surface. No significant differences in water structure were observed on the ALD-Al_2O_3, -ZrO_2, and CoO films/Co foil, aside from an approximately fivefold reduction in intensity on CoO, which was attributed to scattering losses caused by the sub-micron scale rough CoO film/Co foil surface. In contrast, for CO adsorption on rough Ir surfaces (on the nanometer scale), as compared to smooth Ir(111), an eightfold enhancement in SFG intensity has been observed due to a light-induced excitation of localized surface plasmon resonances[75].

These findings underscore the importance of oxide surface structure in governing water adsorption behavior. Previous studies have demonstrated that water dissociation is enhanced on ultrathin MgO films compared to bulk-like MgO(001)[60], motivating further investigation of thickness-dependent SFG responses in ALD-grown Al_2O_3, ZrO_2, and TiO_2 films. For MgO(001)/Ag(001)[60], SFG measurements indicated that films exhibit bulk-like characteristics at thicknesses as small as 3 ML. At the liquid D_2O-TiO_2 interface (with TiO_2 deposited by ALD on a CaF_2 window), SFG spectra showed that the differences between samples with 85 vs. 150 nm TiO_2 film were independent of film thickness[67]. Extending similar investigations to ALD oxides may yield valuable insights for designing surfaces with reduced ice adhesion.

Open Access Article. Published on 16 Dezember 2025. Downloaded on 04.04.2026 08:28:47.
This article is licensed under a Creative Commons Attribution 3.0 Unported Licence.

Experimental methods

Sample preparation

- **ALD-grown oxide films**

The Sieger Wafer SiO_2/Si wafter (525 µm N-type, phosphorus-doped, <100>, 1-5 Ω) (7x7 mm^2) was used as the substrate for atomic layer deposition (ALD). Before deposition, the Si wafers were sonicated in acetone and methanol to remove glue residues and then dried in N_2. Al_2O_3 and TiO_2 thin films were deposited onto the Si substrate using thermal-mode ALD in an R-200 standard reactor (Picosun, Finland). ZrO_2 films were grown using a Gemstar thermal ALD system (Arradiance, LLC).

Al_2O_3 films were prepared using alternating exposures of trimethylaluminum (TMA, EpiValence) (Al precursor) and H_2O (EpiValence). Each ALD cycle consisted of a pulse-purge sequence: 0.1 s TMA pulse, 5 s N_2 purge, 0.1 s H_2O pulse, and 8 s N_2 purge. TMA was stored in a stainless-steel bubbler maintained at 22 °C. The reaction chamber temperature was set to 150 °C and the chamber pressure to 9 hPa. In all cases, the H_2O reservoir was kept at 22 °C, and the ultrahigh purity nitrogen (Messer Technogas, 99.999%) was used as the carrier and purge gas. A total of 40 ALD cycles were performed.

Faraday Discussions Accepted Manuscript

View Article Online
DOI: 10.1039/D5FD00152H

ZrO_2 films were deposited using tetrakis(dimethylamino)zirconium(IV) (TDMAZ, Sigma-Aldrich) and deionized H_2O. The manifolds and chamber temperatures were maintained at 140 °C. N_2 (99.999%) was used as carrier gas at a flow of 50 SCCM. The TDMAZ bubbler was kept at 75 °C and the H_2O bubbler at room temperature. The TDMAZ and H_2O pulse/purge times were 50 ms/12 s and 100 ms/12 s per ALD cycle, respectively. A total of 35 ALD cycles were performed.

TiO_2 films were deposited using tetrakis(dimethylamido)titanium(IV) (TDMATi from Strem Chemicals) and H_2O (EpiValence). The TDMATi was evaporated at 85 °C. The substrate temperature was 150 °C and the chamber pressure was 1 kPa during deposition. One TiO_2 ALD cycle consisted of a 1.6 s TDMATi pulse, 6 s N_2 purge, 0.1 s H_2O pulse, and 8 s N_2 purge. A total of 83 ALD cycles were performed.

- **CoO oxide film**

A polycrystalline cobalt foil (1 x 1 cm^2, 99.9% purity, MaTecK GmbH) was cleaned according to the procedure described by Wu et al. [83] to obtain a contaminant-free Co surface. The effectiveness of the cleaning process was verified by XPS and LEIS. The cleaned foil was subsequently oxidized by annealing in an oxygen atmosphere (pO_2 = 1x10^{-6} mbar) at 300 °C for 5 h, until the absence of metallic Co signals in the XPS spectrum confirmed complete oxidation of the near-surface region of the polycrystalline Co foil. After oxidation, a LEIS spectrum was recorded.

- **D_2O ice**

D_2O ice was prepared by water vapor deposition. D_2O was exposed to the chamber after a freeze-thaw cycle.

Ellipsometry

The oxide thickness was determined by spectroscopic ellipsometry using an EP4 imaging ellipsometer (Accurion GmbH) equipped with a 10× objective and a 50° angle of incidence, over the spectral range 360–1000 nm (filter-wheel configuration with 45 wavelengths).

X-ray photoelectron spectroscopy (XPS) and low-energy ion scattering (LEIS)

XPS and LEIS were conducted in a dedicated ultra-high-vacuum chamber (UHV 1) (35 L) with a base pressure ≤ 5x10^{-10} mbar. As described in ref[84, 85], the system was equipped with a high-intensity, non-monochromatic Al/Mg dual-anode X-ray source (XR50, SPECS GmbH) and a hemispherical energy analyzer (Phoibos 100©) with a multichannel plate detector. For ALD-grown oxides, Al Kα radiation (1486.61 eV) was used for the acquisition of XPS spectra. For CoO film, Mg Kα radiation (1253.6 eV) was used with an emission angle of 0° and an analyzer pass energy of 20 eV. All XPS spectra were acquired at room temperature. Before XPS, all samples were thoroughly cleaned by a cycle of oxidation (1x10^{-6} mbar O_2, 923 K, 30 min) and reduction (1x10^{-6} mbar H_2, 923 K, 30 min).

Open Access Article. Published on 16 Dezember 2025. Downloaded on 04.04.2026 08:28:47.
This article is licensed under a Creative Commons Attribution 3.0 Unported Licence.

Faraday Discussions Accepted Manuscript

LEIS measurements were performed using a SPECS IQE 12/38© ion source operated with He^+ ions at a kinetic energy of 1 keV, a helium backpressure of 2 x 10^{-7}mbar, and a scattering angle of 135°.

View Article Online
DOI: 10.1039/D5FD00152H

SFG spectroscopy

The SFG cell can be operated from 2.5 × 10^{-8} mbar to 1 bar pressure and at 100−800 K[75, 86, 87]. SFG measurements were performed using a 20 ps mode-locked Nd:YAG laser system (EKSPLA, PL2241) with a fundamental radiation of 1064 nm (30 mJ/pulse, 50 Hz repetition rate)[86]. A tunable mid-infrared beam (with the photon energy ωIR) and a visible beam with a fixed wavelength of 532 nm were directed in a co-propagation geometry toward the surface, with incidence angles of 55° and 58.5° with respect to the surface normal, respectively. The pulse energy was 90−130 μJ for infrared between 2150 and 3800 cm^{-1} and 30 ± 5 μJ for visible. The SFG signal was collected/detected in the reflection direction with a photomultiplier tube (PMT). The polarization of IR was kept as P and that of visible and SFG signal was switched between P and S using a Glan−Taylor prism and a half-wave plate. All spectra were normalized by the energy of visible and IR laser pulses.
Before SFG measurements (in UHV 2), all oxide films were oxidized in 1x10^{-5} mbar O_2 at 600 K for 60 min. If SFG measurements could not be finished on the same day, the next day samples were only annealed at 423 K for 30 min under UHV only to remove adsorbed H_2O (traces in the UHV chamber).

Open Access Article. Published on 16 Dezember 2025. Downloaded on 04.04.2026 08:28:47.
This article is licensed under a Creative Commons Attribution 3.0 Unported Licence.

Author contributions

X.L. carried out the original draft writing, the conception and design of this study, and the SFG experiments and data acquisition. S.G., T.H., Š.V., and G.R. participated in manuscript preparation.
M.-H.J. and Y.L. prepared ALD-ZrO_2 films and M.Z. prepared ALD-Al_2O_3 and TiO_2 films. S.G. performed the LEIS + XPS measurements of the CoO films. T.H. performed the XPS measurements for all ALD films. M.-H.J. and M.J. performed ellipsometry on ALD films. J.E.O. participated in the XPS and SFG measurements. G.R. contributed to the conception and design of this study and to writing – review and editing. X.L., Š.V. and G.R. contributed to funding acquisition.

Conflicts of interest

There are no conflicts of interest to declare.

Acknowledgements

This research was funded in part by the Austrian Science Fund (FWF) [10.55776/ESP266, 10.55776/F8100, 10.55776/COE5] (ESPRIT, SFB TACO P08, Cluster of Excellence MECS). For open access purposes, the author has applied a CC BY public copyright license to any author accepted manuscript version arising from this submission. M.J., J.E.O. and S.V. acknowledge funding by a grant

Faraday Discussions Accepted Manuscript

View Article Online
DOI: 10.1039/D5FD00152H

from the Programme Johannes Amos Comenius under the Ministry of Education, Youth and Sports of the Czech Republic CZ.02.01.01/00/22_008/0004558 Advanced MUltiscaLe materials for key Enabling Technologies. J.E.O. and S.V. acknowledge the support provided by the project funded by the European Union under Horizon Europe (project 101079142) in the initial exploratory phase of the study. Y.L. acknowledges support from the Fulbright U.S. Scholar Program and the Czech Fulbright Commission.

Open Access Article. Published on 16 Dezember 2025. Downloaded on 04.04.2026 08:28:47.
This article is licensed under a Creative Commons Attribution 3.0 Unported Licence.

References

[1] D. S. Newsome. *Catal. Rev.* 1980, **21**, 275–318. https://doi.org/10.1080/03602458008067535.

[2] C. Ratnasamy; J. P. Wagner. *Catal. Rev.* 2009, **51**, 325–440. https://doi.org/10.1080/01614940903048661.

[3] T. Wang; M. D. Porosoff; J. G. Chen. *Catal. Today* 2014, **233**, 61–69. https://doi.org/10.1016/j.cattod.2013.09.037.

[4] J. Chang; Z. Feng; J. M. Vohs; R. J. Gorte. *Catalysts* 2022, **12**, 1364. https://doi.org/10.3390/catal12111364.

[5] D.-W. Jeong; W.-J. Jang; J.-O. Shim; W.-B. Han; H.-S. Roh; U. H. Jung; W. L. Yoon. *Renew. Energy* 2014, **65**, 102–107. https://doi.org/10.1016/j.renene.2013.07.035.

[6] S. Sá; H. Silva; L. Brandao; J. M. Sousa; A. Mendes. *Appl. Catal. B-Environ.* 2010, **99**, 43–57. https://doi.org/10.1016/j.apcatb.2010.06.015.

[7] P. Nikolaidis; A. Poullikkas. *Renew. Sust. Energ. Rev.* 2017, **67**, 597–611. https://doi.org/10.1016/j.rser.2016.09.044.

[8] D. Yadav; X. L. Lu; C. B. Vishwakarma; D. W. Jing. *J. Power Sources* 2023, **585**, 233621. https://doi.org/10.1016/j.jpowsour.2023.233621.

[9] S. Zhao; F. Chen; S. Duan; B. Shao; T. Li; H. Tang; Q. Lin; J. Zhang; L. Li; J. Huang; et al. *Nat. Commun.* 2019, **10**, 3824. https://doi.org/10.1038/s41467-019-11871-w.

[10] S. Lee; L. M. Molina; M. J. López; J. A. Alonso; B. Hammer; B. Lee; S. Seifert; R. E. Winans; J. W. Elam; M. J. Pellin; et al. *Angew. Chem. Int. Ed.* 2009, **48**, 1467–1471. https://doi.org/10.1002/anie.200804154.

[11] W. Li; J. Shi; P. L. Tangpakonsab; B. Zhang; T. Haunold; A. Genest; N. Yigit; L. Atzl; E. Kokkonen; Y. Qin; et al. *ACS Catal.* 2025, 20496–20511. https://doi.org/10.1021/acscatal.5c05829.

[12] S. J. Tauster. *Acc. Chem. Res.* 1987, **20**, 389–394. https://doi.org/10.1021/ar00143a001.

Faraday Discussions Accepted Manuscript

View Article Online
DOI: 10.1039/D5FD00152H

[13] N. Iwasa; S. Kudo; H. Takahashi; S. Masuda; N. Takezawa. *Catal. Lett.* 1993, **19**, 211–216. https://doi.org/10.1007/BF00771756.

[14] G. E. Brown; V. E. Henrich; W. H. Casey; D. L. Clark; C. Eggleston; A. Felmy; D. W. Goodman; M. Grätzel; G. Maciel; M. I. McCarthy; et al. *Chem. Rev.* 1999, **99**, 77–174. https://doi.org/10.1021/cr980011z.

[15] M. A. Henderson. *Surf. Sci. Rep.* 2002, **46**, 1–308. https://doi.org/10.1016/S0167-5729(01)00020-6.

[16] A. Verdaguer; G. M. Sacha; H. Bluhm; M. Salmeron. *Chem. Rev.* 2006, **106**, 1478–1510. https://doi.org/10.1021/cr040376l.

[17] G. E. Ewing. *Chem. Rev.* 2006, **106**, 1511–1526. https://doi.org/10.1021/cr040369x.

[18] Y. J. Chabal. *Vibrational Properties at Semiconductor Surfaces and Interfaces*; Springer Berlin Heidelberg, 1987.

[19] Y. R. Shen. *The Principles of Nonlinear Optics*; Wiley-Interscience, 1984.

[20] Y. R. Shen. Interfacial liquid structures. In *Fundamentals of Sum-Frequency Spectroscopy*, Cambridge Molecular Science, Cambridge University Press, 2016; pp 145–196.

[21] Y. R. Shen. *Second Harmonic and Sum-Frequency Spectroscopy*; World Scientific, 2023.

[22] X. Li; G. Rupprechter. *Surf. Sci. Rep.* 2024, **79**, 100645. https://doi.org/10.1016/j.surfrep.2024.100645.

[23] E. Vesselli. *J. Phys. Materials* 2020, **3**, 022002. https://doi.org/10.1088/2515-7639/ab7ab2.

[24] E. Vesselli. *Nanoscale Adv.* 2021, **3**, 1319–1330. https://doi.org/10.1039/d0na00827c.

[25] G. Rupprechter. Surface vibrational spectroscopy on noble metal catalysts from ultrahigh vacuum to atmospheric pressure. In *Annual Reports on the Progress of Chemistry, Section C (Physical Chemistry)*, Royal Chem Soc Press, 2004; pp 237–311.

[26] G. Rupprechter; H.-J. Freund. *Top. Catal.* 2001, **14**, 3–14. https://doi.org/10.1023/A:1009094613850.

[27] F. Tang; T. Ohto; S. Sun; J. R. Rouxel; S. Imoto; E. H. G. Backus; S. Mukamel; M. Bonn; Y. Nagata. *Chem. Rev.* 2020, **120**, 3633–3667. https://doi.org/10.1021/acs.chemrev.9b00512.

[28] P. A. Thiel; T. E. Madey. *Surf. Sci. Rep.* 1987, **7**, 211–385. https://doi.org/10.1016/0167-5729(87)90001-X.

[29] S. M. Piontek; E. Borguet. *Surf. Sci. Rep.* 2023, **78**, 100606. https://doi.org/10.1016/j.surfrep.2023.100606.

[30] E. H. G. Backus; J. Schaefer; M. Bonn. *Angew. Chem. Int. Ed.* 2021, **60**, 10482–10501. https://doi.org/10.1002/anie.202003085.

Open Access Article. Published on 16 Dezember 2025. Downloaded on 04.04.2026 08:28:47.
This article is licensed under a Creative Commons Attribution 3.0 Unported Licence.

Faraday Discussions Accepted Manuscript

View Article Online
DOI: 10.1039/D5FD00152H

[31] S. Singla; E. Anim-Danso; A. E. Islam; Y. Ngo; S. S. Kim; R. R. Naik; A. Dhinojwala. *ACS Nano* 2017, **11**, 4899–4906. https://doi.org/10.1021/acsnano.7b01499.

[32] Y. Xu; Y. B. Ma; F. Gu; S. S. Yang; C. S. Tian. *Nature* 2023, **621**, 506–510. https://doi.org/10.1038/s41586-023-06374-0.

[33] Y. Wang; F. Tang; X. Yu; T. Ohto; Y. Nagata; M. Bonn. *Angew. Chem. Int. Ed.* 2024, **63**, e202319503. https://doi.org/10.1002/anie.202319503.

[34] Y. M. Hong; J. L. He; C. Y. Zhang; X. P. Wang. *J. Phys. Chem. C* 2022, **126**, 1471–1480. https://doi.org/10.1021/acs.jpcc.1c08328.

[35] S. M. Piontek; D. Naujoks; T. Tabassum; M. J. DelloStritto; M. Jaugstetter; P. Hosseini; M. Corva; A. Ludwig; K. Tschulik; M. L. Klein; et al. *ACS Phys. Chem. Au* 2023, **3**, 119–129. https://doi.org/10.1021/acsphyschemau.2c00044.

[36] S. Yamaguchi; Y. Suzuki; Y. Nojima; T. Otosu. *Chem. Phys.* 2019, **522**, 199–210. https://doi.org/10.1016/j.chemphys.2019.03.005.

[37] X. Wei; P. B. Miranda; Y. R. Shen. *Phys. Rev. Lett.* 2001, **86**, 1554–1557. https://doi.org/10.1103/PhysRevLett.86.1554.

[38] M. J. Iedema; M. J. Dresser; D. L. Doering; J. B. Rowland; W. P. Hess; A. A. Tsekouras; J. P. Cowin. *J. Phys. Chem. B* 1998, **102**, 9203–9214. https://doi.org/10.1021/jp982549e.

[39] X. Su; L. Lianos; Y. R. Shen; G. A. Somorjai. *Phys. Rev. Lett.* 1998, **80**, 1533–1536. https://doi.org/10.1103/PhysRevLett.80.1533.

[40] W. J. Smit; F. J. Tang; M. A. Sánchez; E. H. G. Backus; L. M. Xu; T. Hasegawa; M. Bonn; H. J. Bakker; Y. Nagata. *Phys. Rev. Lett.* 2017, **119**, 133003. https://doi.org/10.1103/PhysRevLett.119.133003.

[41] L. Wei; Q. Bai; X. Li; Z. Liu; C. Li; Y. Cui; L. Shen; C. Zhu; W. Fang. *J. Phys. Chem. Lett.* 2023, **14**, 8890–8895. https://doi.org/10.1021/acs.jpclett.3c02065.

[42] B.-H. Mao; E. Crumlin; E. C. Tyo; M. J. Pellin; S. Vajda; Y. Li; S.-D. Wang; Z. Liu. *Catalysis Science & Technology* 2016, **6**, 6778–6783. https://doi.org/10.1039/C6CY00575F.

[43] B.-H. Mao; R. Chang; L. Shi; Q.-Q. Zhuo; S. Rani; X.-S. Liu; E. C. Tyo; S. Vajda; S.-D. Wang; Z. Liu. *Phys. Chem. Chem. Phys.* 2014, **16**, 26645–26652. https://doi.org/10.1039/C4CP02325K.

[44] M. Morita. Native Oxide Films and Chemical Oxide Films. In *Ultraclean Surface Processing of Silicon Wafers: Secrets of VLSI Manufacturing*, Hattori, T. Ed.; Springer Berlin Heidelberg, 1998; pp 543–558.

[45] M. Morita; T. Ohmi; E. Hasegawa; M. Kawakami; M. Ohwada. *J. Appl. Phys.* 1990, **68**, 1272–1281. https://doi.org/10.1063/1.347181.

[46] H. J. Mathieu; M. Datta; D. Landolt. *J. Vac. Sci. Technol. A* 1985, **3**, 331–335. https://doi.org/10.1116/1.573260.

Open Access Article. Published on 16 Dezember 2025. Downloaded on 04.04.2026 08:28:47.
This article is licensed under a Creative Commons Attribution 3.0 Unported Licence.

Faraday Discussions Accepted Manuscript

View Article Online
DOI: 10.1039/D5FD00152H

[47] D. Barreca; G. A. Battiston; R. Gerbasi; E. Tondello; P. Zanella. *Surf. Sci. Spectra* 2000, **7**, 303–309. https://doi.org/10.1116/1.1375573.

[48] J. A. Rotole; P. M. A. Sherwood. *Surf. Sci. Spectra* 1998, **5**, 11–17. https://doi.org/10.1116/1.1247851.

[49] U. Diebold; T. E. Madey. *Surf. Sci. Spectra* 1996, **4**, 227–231. https://doi.org/10.1116/1.1247794.

[50] B. R. Strohmeier. *Surf. Interface Anal.* 1990, **15**, 51–56. https://doi.org/10.1002/sia.740150109.

[51] K. Muraoka. *Appl. Phys. Lett.* 2002, **80**, 4516–4518. https://doi.org/10.1063/1.1486046.

[52] S. W. Russell; J. W. Strane; J. W. Mayer; S. Q. Wang. *J. Appl. Phys.* 1994, **76**, 257–263. https://doi.org/10.1063/1.357137.

[53] S. Baldelli; M. Mascal; J. C. Bertran. *Chem. Phys. Lett.* 2006, **427**, 72–75. https://doi.org/10.1016/j.cplett.2006.06.038.

[54] R. R. Feng; A. A. Liu; S. Liu; J. J. Shi; R. D. Zhang; Z. F. Ren. *J. Phys. Chem. C* 2015, **119**, 9798–9804. https://doi.org/10.1021/jp512798f.

[55] M. Nishijima; K. Edamoto; Y. Kubota; S. Tanaka; M. Onchi. *J. Chem. Phys.* 1986, **84**, 6458–6465. https://doi.org/10.1063/1.450741.

[56] M. J. Stirniman; C. Huang; R. Scott Smith; S. A. Joyce; B. D. Kay. *J. Chem. Phys.* 1996, **105**, 1295–1298. https://doi.org/10.1063/1.471993.

[57] C. Codeço; J. Barreto; R. Caetano; G. Fickenscher; G. Felix; J. Libuda; F. Stavale. *J. Phys. Chem. C* 2024, **128**, 19630–19637. https://doi.org/10.1021/acs.jpcc.4c05880.

[58] M. Nagao; K. Watanabe; Y. Matsumoto. *J. Phys. Chem. C* 2009, **113**, 11712–11719. https://doi.org/10.1021/jp901793q.

[59] W. Gan; D. Wu; Z. Zhang; R. R. Feng; H. F. Wang. *J. Chem. Phys.* 2006, **124**, 114705. https://doi.org/10.1063/1.2179794.

[60] E. Carrasco; M. A. Brown; M. Sterrer; H. J. Freund; K. Kwapien; M. Sierka; J. Sauer. *J. Phys. Chem. C* 2010, **114**, 18207–18214. https://doi.org/10.1021/jp105294e.

[61] H. F. Wang; W. Gan; R. Lu; Y. Rao; B. H. Wu. *Int. Rev. Phys. Chem.* 2005, **24**, 191–256. https://doi.org/10.1080/01442350500225894.

[62] W. J. Smit; F. J. Tang; Y. Nagata; M. A. Sánchez; T. Hasegawa; E. H. G. Backus; M. Bonn; H. J. Bakker. *J. Phys. Chem. Lett.* 2017, **8**, 3656–3660. https://doi.org/10.1021/acs.jpclett.7b01295.

[63] G. Cicero; J. C. Grossman; E. Schwegler; F. Gygi; G. Galli. *J. Am. Chem. Soc.* 2008, **130**, 1871–1878. https://doi.org/10.1021/ja074418+.

[64] N. Aiga; T. Sugimoto; Y. Otsuki; K. Watanabe; Y. Matsumoto. *Phys. Rev. B* 2018, **97**, 075410. https://doi.org/10.1103/PhysRevB.97.075410.

Open Access Article. Published on 16 Dezember 2025. Downloaded on 04.04.2026 08:28:47.
This article is licensed under a Creative Commons Attribution 3.0 Unported Licence.

Faraday Discussions Accepted Manuscript

View Article Online
DOI: 10.1039/D5FD00152H

[65] E. Anim-Danso; Y. Zhang; A. Dhinojwala. *J. Phys. Chem. C* 2016, **120**, 3741–3748. https://doi.org/10.1021/acs.jpcc.5b08371.

[66] Z. Dohnálek; G. A. Kimmel; R. L. Ciolli; K. P. Stevenson; R. S. Smith; B. D. Kay. *J. Chem. Phys.* 2000, **112**, 5932–5941. https://doi.org/10.1063/1.481166.

[67] S. J. Schlegel; S. Hosseinpour; M. Gebhard; A. Devi; M. Bonn; E. H. G. Backus. *Phys. Chem. Chem. Phys.* 2019, **21**, 8956–8964. https://doi.org/10.1039/C9CP01131E.

[68] H. Li; J.-I. J. Choi; W. Mayr-Schmölzer; C. Weilach; C. Rameshan; F. Mittendorfer; J. Redinger; M. Schmid; G. Rupprechter. *J. Phys. Chem. C* 2015, **119**, 2462–2470. https://doi.org/10.1021/jp5100846.

[69] M. Schmid. *LEIS Energy Calculator*. IAP/TU Wien Surface Physics Group 2002-2023, https://www2.iap.tuwien.ac.at/www/surface/leis (accessed 01-11-2025).

[70] S. Průša; M. R. Linford; E. Vaníčková; P. Bábík; J. W. Pinder; T. Šikola; H. H. Brongersma. *Appl. Surf. Sci.* 2024, **657**, 158793. https://doi.org/10.1016/j.apsusc.2023.158793.

[71] M. C. Biesinger; B. P. Payne; A. P. Grosvenor; L. W. M. Lau; A. R. Gerson; R. S. C. Smart. *Appl. Surf. Sci.* 2011, **257**, 2717–2730. https://doi.org/10.1016/j.apsusc.2010.10.051.

[72] T. J. Chuang; C. R. Brundle; D. W. Rice. *Surf. Sci.* 1976, **59**, 413–429. https://doi.org/10.1016/0039-6028(76)90026-1.

[73] F. Buchner; K. Forster-Tonigold; J. Kim; J. Bansmann; A. Groß; R. J. Behm. *Chem. Mater.* 2019, **31**, 5537–5549. https://doi.org/10.1021/acs.chemmater.9b01253.

[74] M. Hassel; H. J. Freund. *Surf. Sci. Spectra* 1996, **4**, 273–278. https://doi.org/10.1116/1.1247797.

[75] X. Li; S. Baronio; S. Gross; T. Haunold; E. Vesselli; G. Rupprechter. *J. Phys. Chem. C* 2025, **129**, 12551–12560. https://doi.org/10.1021/acs.jpcc.5c02545.

[76] S. Baldelli; A. S. Eppler; E. Anderson; Y. R. Shen; G. A. Somorjai. *J. Chem. Phys.* 2000, **113**, 5432–5438. https://doi.org/10.1063/1.1290024.

[77] C. Y. Wang; H. Groenzin; M. J. Shultz. *J. Am. Chem. Soc.* 2005, **127**, 9736–9744. https://doi.org/10.1021/ja051996m.

[78] C.-y. Wang; H. Groenzin; M. J. Shultz. *Langmuir* 2003, **19**, 7330–7334. https://doi.org/10.1021/la0345542.

[79] J. J. Yang; E. G. Wang. *Phys. Rev. B* 2006, **73**, 035406. https://doi.org/10.1103/PhysRevB.73.035406.

[80] G. V. Franks; Y. Gan. *J. Am. Ceram. Soc.* 2007, **90**, 3373–3388. https://doi.org/10.1111/j.1551-2916.2007.02013.x.

[81] K. Uosaki; T. Yano; S. Nihonyanagi. *J. Phys. Chem. B* 2004, **108**, 19086–19088. https://doi.org/10.1021/jp045173f.

Open Access Article. Published on 16 Dezember 2025. Downloaded on 04.04.2026 08:28:47.
This article is licensed under a Creative Commons Attribution 3.0 Unported Licence.

Faraday Discussions Accepted Manuscript

[82] X. Li; J. C. Liu; K. Lin; Y. Zhang; Y. H. Zhang; R. H. Zheng; Q. Shi; Y. Guo; Z. Lu. *J. Phys. Chem. C* 2019, **123**, 12975–12983. https://doi.org/10.1021/acs.jpcc.9b04044.

View Article Online
DOI: 10.1039/D5FD00152H

[83] C. H. Wu; B. Eren; H. Bluhm; M. B. Salmeron. *ACS Catal.* 2017, **7**, 1150–1157. https://doi.org/10.1021/acscatal.6b02835.

[84] T. Haunold; G. Rupprechter. *Surf. Sci.* 2021, **713**, 121915. https://doi.org/10.1016/j.susc.2021.121915.

[85] M. Roiaz; L. Falivene; C. Rameshan; L. Cavallo; S. M. Kozlov; G. Rupprechter. *J. Phys. Chem. C* 2019, **123**, 8112–8121. https://doi.org/10.1021/acs.jpcc.8b07668.

[86] M. Roiaz; V. Pramhaas; X. Li; C. Rameshan; G. Rupprechter. *Rev. Sci. Instrum.* 2018, **89**, 045104. https://doi.org/10.1063/1.5021641.

[87] V. Pramhaas; H. Unterhalt; H.-J. Freund; G. Rupprechter. *Angew. Chem. Int. Ed.* 2023, **62**, e202300230. https://doi.org/10.1002/anie.202300230.

Open Access Article. Published on 16 Dezember 2025. Downloaded on 04.04.2026 08:28:47.
This article is licensed under a Creative Commons Attribution 3.0 Unported Licence.

Faraday Discussions Accepted Manuscript

Data Availability Statement

View Article Online
DOI: 10.1039/D5FD00152H

The data supporting this article have been included as part of the Supplementary Information. Supplementary information: XPS data fitting information, Figures S1, S5 and S6 are XPS spectra; Figure S4 is a LEIS spectrum; Figures S2, S3, S7, and S9 are SFG spectra and Figure S8 shows photographs of samples.

Open Access Article. Published on 16 Dezember 2025. Downloaded on 04.04.2026 08:28:47.
This article is licensed under a Creative Commons Attribution 3.0 Unported Licence.

Faraday Discussions Accepted Manuscript